scientific reports

Check for updates

OPEN

Murine colon cancer derived cells exhibit heterogeneous resistance profiles against an oncolytic virus

Alejandra Larrieux & Rafael Sanjuán✉

Oncolytic virotherapy has shown efficacy in various animal models and a few human cancers. However, there are still significant limitations for the implementation of these therapies. One such limitation is the emergence of cellular resistances, which may appear rapidly considering the high genetic heterogeneity of most tumors. We previously showed that cellular resistance to an oncolytic virus can be mediated by the chronic activation of innate immunity. Here, we explored the existence of additional resistance mechanisms in murine colon cancer-derived cells. For this purpose, we isolated two cellular clones that were resistant to the oncolytic virus VSV-D51. While one of the clones showed a strong resistance profile associated with increased cytokine-mediated antiviral responses, the other clone showed a lower level of resistance that involves cytoskeletal reorganization, signaling by small GTPases, and cell structural changes. These results demonstrate the capacity of tumor cells to deploy heterogeneous mechanisms of resistance to oncolytic viruses.

Keywords Oncolytic virus, Vesicular stomatitis virus, Cellular resistance, Antiviral response, Innate immunity

Oncolytic viruses are promising biotherapies that exploit cellular vulnerabilities to selectively infect and replicate within tumor cells, while exempting healthy cells from the infectious process[1–3]. An extensive body of experimental evidence, conducted using both natural and engineered oncolytic viruses, such as vesicular stomatitis virus (VSV), adenovirus, herpes simplex virus, and Newcastle disease virus, among others, supports the efficacy of this therapeutic approach[4]. However, as other cancer therapies, oncolytic virotherapies encounter resistance challenges, including antibody and cellular responses[5], interferon (IFN)-mediated resistance[6,7], epigenetic modifications[8,9], inactivation of cell death mechanisms, insensitivity to growth suppressor signals, and spatial barriers[10,11], among many others[12]. For instance, many oncolytic viruses are particularly sensitive to interferon (IFN)-mediated cellular antiviral responses, and their efficacy is thus dependent on the degree of disruption of IFN signaling shown by target cells[13]. Unfortunately, a significant percentage of tumor cells retain intact IFN signaling, as well as constitutive expression of IFN-stimulated genes (ISGs) and resistance gene signatures[14–17]. Therefore, the emergence of immune-based cellular resistance in populations initially susceptible to infection represents a barrier to the development of oncolytic viruses and determines their efficacy[10,16–18].

VSV, a member of the *Rhabdoviridae* family, is a single-stranded negative-sense RNA virus with a relatively small genome size (11.2 kb), encoding five genes: nucleocapsid (N), phosphoprotein (P), glycoprotein (G), matrix protein (M), and polymerase (L). Over the past two decades, VSV has been extensively used as a platform for the development of oncolytic viruses due to its broad cellular tropism, lack of human immunity, and extensive knowledge about its genome and infection cycle[19,20]. A highly-studied oncolytic VSV is the attenuated variant VSV-D51 (also referred to as VSVΔ51 M) which carries a deletion of methionine 51 in the M protein[20–22]. This mutation abolishes the ability of the M protein to inhibit cellular gene expression, a function that the wild-type variant achieves by blocking nuclear export of mRNAs. Consequently, normal cells can mount an antiviral response and are resistant to infection by VSV-D51. In contrast, most tumor cells have defects in their innate immune responses and remain susceptible to this attenuated virus. Thus, although VSV-D51 infects a wide range of cell lines[20], it exhibits limited efficacy in cell lines with intact innate immune response mechanisms[14,23,24]. In a previous study, we showed that the chronic activation of innate immunity is a powerful cellular resistance mechanism against VSV-D51 in mouse melanoma cells[16].

In the present study, we explored the emergence of resistances to VSV-D51 in CT26 cells, a mouse carcinoma cell line initially susceptible to VSV infection. Our previous results suggested that certain CT26 clones have evolved resistance mechanisms similar to those previously observed in melanoma cells, whereas other CT26

Institute for Integrative Systems Biology (I2SysBio), Universitat de València-CSIC, Paterna 46980, València, Spain. ✉email: rafael.sanjuan@uv.es

clones may show different mechanisms. Here, we demonstrated the heterogeneity of CT26 cells in relation to VSV infection susceptibility in terms of viral kinetics, breadth of resistance against different VSV variants, cytokine responsiveness, and transcriptomics.

Results

Resistance to VSV-D51 is partial and heterogeneous among CT26 cells

In a previous study focused on B16 mouse melanoma cells[16], we also reported the emergence of resistances against VSV-D51 in CT26 mouse colon carcinoma cells. We found that VSV-D51 triggered massive death of CT26 cells but that a fraction of the cells survived and remained refractory to subsequent challenge with VSV-D51. We used cell sorting to isolate two CT26-derived clones (C1 and C4) from the surviving fraction and checked that the amplified clones were completely free of VSV by RT-qPCR and titration. Quantitation of the GFP signal (reporter encoded by VSV-D51), titrations at 24 h post-infection (hpi), and RT-qPCR to detect viral RNA showed that both clones were less susceptible to VSV-D51 than the original (naïve) CT26 cells, although 24 hpi titers in C4 did not differ significantly from those obtained in naïve CT26 cells. These previous data are summarized in Fig. 1. In the present work, to better examine differences in viral production between C1, C4 and naïve CT26 cells, we also titrated infected cultures at 8 hpi. This revealed slower viral production in the C4 clone compared to naïve cells (Fig. 1b). In our previous work, we also carried out an RNAseq analysis of uninfected C1, C4 and naïve CT26 cells to test whether gene expression profiles associated to VSV-D51 resistance were similar in CT26 and B16 cells. The results showed a strong positive correlation between the differentially expressed genes (DEGs) in all B16-resistant clones and the CT26 clone C1. The activation of the Janus kinase/signal transducer and activator of transcription (JAK/STAT) signaling pathway (Supplementary Fig. S1), which specifically controls ISG transcription through IFN signaling, together with the immune-related nature of the identified genes, suggested that chronic activation of immune response mechanisms could be a general mechanism of resistance to attenuated VSV in tumor cells. However, another CT26 clone, C4, showed a very weak correlation with C1 (Fig. 1e), and no similarities in DEGs with B16-resistant clones[16]. Here, we confirmed that C4 phenotype diverges from chronic immune response activation (Fig. 1f), instead exhibiting increased cytoskeleton reorganization, small GTPase/Ras signal transduction, and an enhanced response to

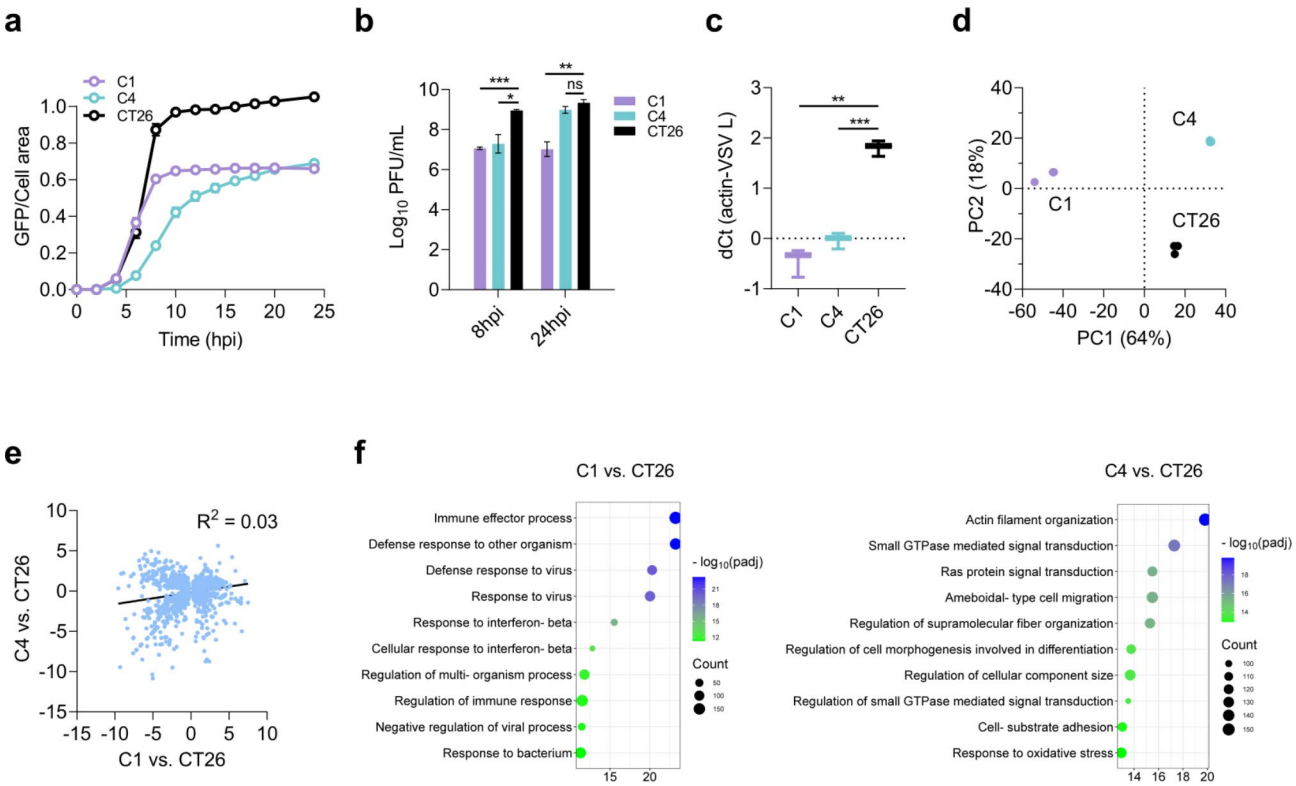

Fig. 1. VSV-D51 resistance in C1, C4 and naïve CT26 cells. (**a**) Normalized GFP fluorescence curves vs. time of VSV-D51 infection (MOI = 0.1 PFU/cell) in C1, C4, and naïve CT26 cells. **(b)** Viral progeny production (Log_{10} PFU/mL) at 8 and 24 hpi (VSV-D51, MOI = 0.1 PFU/cell). **(c)** Relative viral RNA expression at 8 hpi (VSV-D51, MOI = 0.1 PFU/cell). **(d)** Principal component analysis of global gene expression in uninfected C1, C4, and naïve CT26 cells. **(e)** Correlation of differentially expressed genes (DEGs) shared in C1 vs. CT26 and C4 vs. CT26 ($P < 0.001$). **(f)** Top ten of the most enriched Gene Ontology (GO) pathways in C1 vs. CT26 and C4 vs. CT26. In a-c figures, experimental data are presented as the mean ± SEM of each observation, and asterisks indicate significant differences compared to naïve CT26 cells using Welch's t-tests.

oxidative stress. These results indicate that VSV resistance in CT26 cells may be underpinned by more than one cellular mechanism.

Susceptibility to wild-type VSV

Quantitative real-time fluorescence microscopy showed that wild-type VSV infection progressed more slowly in C1 cells than in naïve CT26 cells, whereas no such differences were found for C4 cells (Fig. 2). We also found reduced viral titer at both 8 hpi and 24 hpi (Welch's t-tests: $P<0.001$) and lower viral RNA signal production at 8 hpi ($P=0.006$) in C1 cells, but not in C4 cells. This discrepancy in wild-type VSV susceptibility between the clones suggests that infection resistance mechanisms may be different, being specific to the attenuated variant VSV-D51 in the case of the C4 population.

Cytokine-mediated responses to infection

We stimulated the production of cytokines and antiviral factors in C1, C4 and naïve CT26 cells by infecting them with VSV-D51. After filtering the infection supernatant to remove viral progeny as previously described[16], we pre-treated fresh cell monolayers with these conditioned media and infected them with VSV-D51. The effect of this treatment on infection was quantified using GFP areas and titers. Both C1 and C4 clones demonstrated robust responses to their own antiviral-conditioned media, as evidenced by a significant reduction in 24 hpi GFP signal and in viral titer in pre-treated cells compared to untreated controls, particularly for C1 cells (Welch's t-tests: $P<0.01$, Fig. 3). In contrast, naïve CT26 cells exhibited a limited response to their own conditioned media, showing a marginally significant drop in GFP signal at 24 hpi ($P=0.04$) but no deviations in viral titer. Both indicators dropped slightly more but still modestly when naïve CT26 cells were pre-treated with conditioned media obtained from C1 and C4. Finally, C1 and C4 cells exhibited diminished viral titer and GFP signal when pre-treated with conditioned medium obtained from naïve CT26 cells (Welch's t-tests: $P<0.03$). Altogether, these results indicated that the less-permissive CT26 clones C1 and C4 showed augmented antiviral cytokine signaling compared to naïve CT26, both in terms of cytokine production and responsiveness.

Basal gene expression profiles

To better understand the basis of reduced sensitivity to VSV-D51 in these cells, we examined their basal transcriptomic profiles relative to naïve CT26 cells (i.e., in the absence of VSV infection). This revealed massive differences between clones C1 and C4 (Fig. 4a and b). The C1 cells overexpressed IFN genes, cytokines, and multiple ISGs (Fig. 4c), along with a marked immune-enhanced and antiviral response profile (Fig. 4d). In contrast, K-means clustering indicated that the most overexpressed genes in C4 cells were associated with cellular Gene Ontology (GO) processes related to cell morphogenesis, cytoskeletal reorganization, cell surface receptor signaling and cell adhesion, with no evidence of immune mechanisms involved (Fig. 4e). The detection of intracellular viral RNA following WT and D51 infection, coupled with the absence of differences in the expression of the principal VSV receptor (low-density lipoprotein receptor gene, *Ldlr*) and the unaltered ability of VSV to adhere to the cell surface (Supplementary Fig. S2), ruled out the possibility that the reduced infectivity in C1 and C4 cells was due to lower receptor availability. These results highlight the differences between resistant CT26-derived clones, not only in comparison to naïve CT26 cells but also among themselves, and suggest that mechanisms beyond chronic activation of the immune response are involved in resistance to oncolytic VSV.

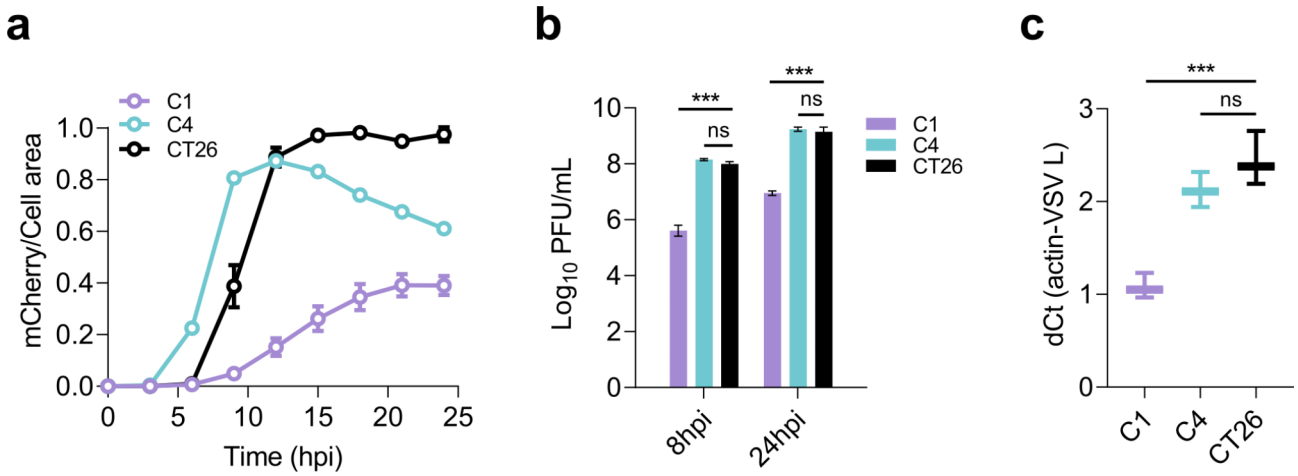

Fig. 2. Wild-type VSV resistant profile of C1, C4 and naïve CT26 cells. (**a**) Normalized mCherry fluorescence curves vs. time of VSV-WT infection (MOI = 0.1 PFU/cell) in C1, C4, and CT26 cells. The declining signal observed for C4 cells was probably due to virus-induced cell death from infection, as cell detachment occurred faster in C4 (18–24 hpi) than in naïve CT26 cells (20–24 hpi). **(b)** Viral progeny production (Log_{10} PFU/mL) at 8 and 24 hpi. **(c)** Relative viral RNA expression at 8 hpi. Asterisks indicate significant differences compared to naïve CT26 cells by Welch's t-tests.

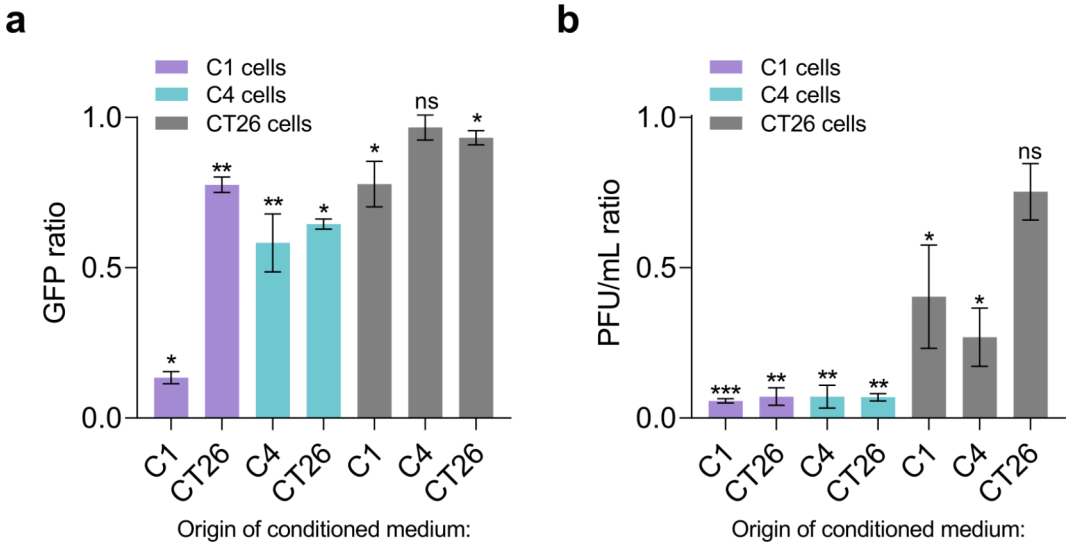

Fig. 3. Cytokine-mediated responses in C1, C4, and naïve CT26 cells. (**a**) GFP signal ratio at 24 hpi (treated/untreated) of C1, C4, and naïve CT26 cells that were previously treated or not with virus-free media collected from a prior infection and then inoculated with VSV-D51 (MOI = 0.1 PFU/cell). **(b)** VSV-D51 titers ratio after 24 hpi from (A). In both figures, asterisks indicate significant differences between the treated and untreated values for each condition using Welch's t-tests.

Transcriptomic responses to VSV-D51 infection

We then aimed to analyze the transcriptomic changes following VSV-D51 infection. Initial exploratory analysis confirmed the differences in VSV infection response among C1, C4 and naïve CT26 infected cells (Fig. 5a and c). As expected, naïve CT26 cells showed upregulation of IFN and cytokine expression after infection (Fig. 5d; Supplementary Table 3). A comparison of C4 and naïve CT26 infected/uninfected DEGs showed strong co-expression (Fig. 5e), suggesting that the response to VSV may be articulated similarly. As in naïve CT26 cells, components of the IFN-mediated antiviral response, cytokines, and ISGs were among the most overexpressed genes in C4-infected cells (Supplementary Table 4). However, the total number of DEGs was almost double in naïve CT26 cells than in C4-infected cells, suggesting that VSV infection stimulates smaller-scale gene reprogramming in the latter.

Conversely, DEGs shared between infected and uninfected C1 and naïve CT26 cells were uncorrelated, as C1-uninfected cells chronically overexpress IFN and antiviral components. C1 cells showed less than 100 DEGs following VSV-D51 infection, which contrasts with the over 5000 DEGs detected in C4 cells. Furthermore, C1 and C4 shared only 11 DEGs, their degree of change being uncorrelated. In C1 cells, the most dysregulated genes after VSV infection were mostly non-coding or experimentally unconfirmed genes (Supplementary Table 5). Moreover, only two coding genes, Nitric oxide synthase 2 (*Nos2*) and NADPH quinone oxidoreductase 1 (*Nqo1*), appeared to be more than twice under-expressed after infection. Deregulated genes in infected C1 cells did not significantly enrich any functional processes included in the GO, Kyoto Encyclopedia of Genes and Genomes (KEGG; https://www.kegg.jp/kegg/kegg1.html), Reactome, or WikiPathway databases. This lack of significance may be attributed to the fact that, of the 98 DEGs, only 22 correspond to protein-coding genes. Proteins encoded by these genes also interacted very weakly (STRING PPI: $P = 0.551$). In contrast, significant enrichment was found in GO processes related to cellular response to viruses, response to IFN, and chromatin modification in C4-infected cells (Fig. 5f). KEGG analyses confirmed the overrepresentation of viral regulatory processes such as apoptosis, Tumor necrosis factor (TNF) signaling, and viral infections such as hepatitis C, Epstein-Barr, and human papillomavirus (HPV), likely due to the overrepresentation of master regulatory genes, such as *Stat2* or *Jak1*, which participate in common cellular regulation against viral infection.

Validation of the RNAseq results by qPCR

To validate the results obtained from the RNAseq analyses, three differentially regulated genes in each cell line and infection condition were selected for qPCR analysis. For comparison between C1 and C4, we analyzed the expression of the immune-related genes IFN regulatory factor 7 (*Irf7*), Mx dynamin-like GTPase 2 (*Mx2*), and 2′-5′-oligoadenylate synthase-like (*Oasl*), previously used[16] (Fig. 6a). For the VSV-D51 infected versus uninfected comparison, we analyzed the expression of the Metastasis associated lung adenocarcinoma transcript 1 (*Malat1*), BarH like homeobox 1 (*Barhl1*), and Leucyl-tRNA synthetase mitochondrial (*Lars2*) genes in C1 cells and Mx dynamin-like GTPase 1 (*Mx1*), Guanylate binding protein 5 (*Gbp5*), and Interferon activated gene 205 (*Ifi205*) in C4 and naïve CT26 cells (Fig. 6b). Comparative analysis of the RNAseq and qPCR data revealed consistent results (Pearson $r = 0.98$, $P < 0.001$, Fig. 6c).

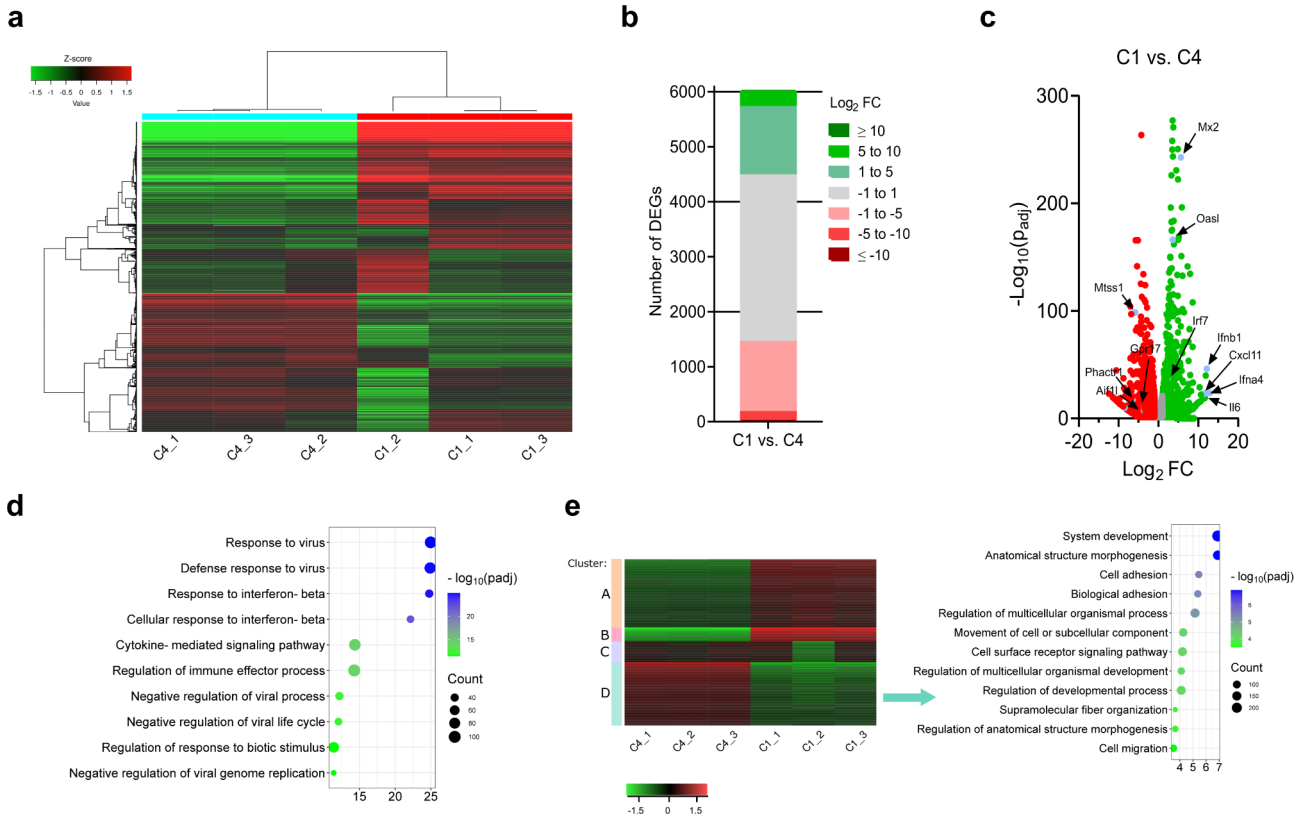

Fig. 4. Transcriptomic differences between clones C1 and C4. (**a**) Hierarchical clustering and heatmap showing the top 1000 most variable genes between C1 and C4 cells (correlation distance, average linkage). The color bar (Z-score) was calculated as follows: $Z = (x - \mu)/\sigma$, where x represents the expression level of a gene in the sample, μ is the mean expression level of that gene across all samples, and σ is the standard deviation of the gene expression levels across the sample dataset. **(b)** Distribution of differentially expressed genes between C1 and C4 with statistical significance ($P_{adj} < 0.05$). **(c)** Volcano plot of differentially expressed genes between C1 and C4. Representative overexpressed components in C1 related to the interferon-mediated antiviral response (*Ifna4* and *Ifnb1*), cytokines (*Il6* and *Cxcl11*), and ISGs (*Mx2*, *Irf7*, *and Oasl*) are indicated by arrows. Representative overexpressed C4-genes (underexpressed in C1) related to actin-cytoskeleton reorganization (*Phactr1*, *Aif1l* and *Mtss1*) and small GTPase signaling transduction (*Gpr17*), are marked. **(d)** Top ten GO processes enriched in C1 cells compared to C4 ($P_{adj} < 0.05$). **(e)** K-means clustering of transcriptomic C1 and C4-uninfected cells data. K-means was used to define four groups of genes with similar expression profiles (1000 most variable genes using correlation distance). On the right, the GO pathways enriched in Cluster D are shown.

Discussion

The success of a viral infection is determined by complex virus-host interactions. This study provides insights into the heterogeneous susceptibility of CT26 mouse colon carcinoma cells to VSV infection. In our previous study, we identified VSV-D51 resistance in CT26 cells[16], isolating two distinct clones, C1 and C4. We found no evidence of a decrease or loss of viral attachment in these clones. The reduced detection of intracellular VSV genomes, along with the lower production of viral progeny, suggests a decrease in the efficiency of viral replication or in the assembly of new virions, rather than a complete inhibition of these processes. Both clones, especially C1, exhibited strong antiviral responses to their own conditioned media, unlike naïve CT26 cells. Transcriptomic analysis revealed that VSV resistance in C1 cells, as well as in previously characterized B16-derived clones, relies on chronic activation of the immune response. In contrast, VSV resistance in C4 cells exhibited a non-immune character, possibly involving cellular structural changes. The dichotomy between C1 and C4 underscores the existence of multiple mechanisms leading to VSV resistance.

The basal overexpression of immune genes in C1 not only reduced its susceptibility to wild-type and attenuated VSV, but also hindered gene expression reprogramming after VSV-D51 infection and amplified its ability to respond effectively to cytokine-mediated antiviral signals, highlighting the integral role of immune pathway activation in mediating viral resistance[12,25]. A significant body of literature supports that intact IFN signaling is mainly responsible for the weak response to oncolytic virotherapy with Semliki Forest virus[26], adenovirus[27], VSV[15,16,23,28], and Sindbis virus[29], among others[6,7,12]. Indeed, reverting chronic activation of the innate immune response through inhibitors of the JAK/STAT pathway, such as ruxolitinib (JAK1/2 inhibitor), has been shown to promote oncolytic viral infection[30–32]. This type of intervention could have practical implications, as chronic

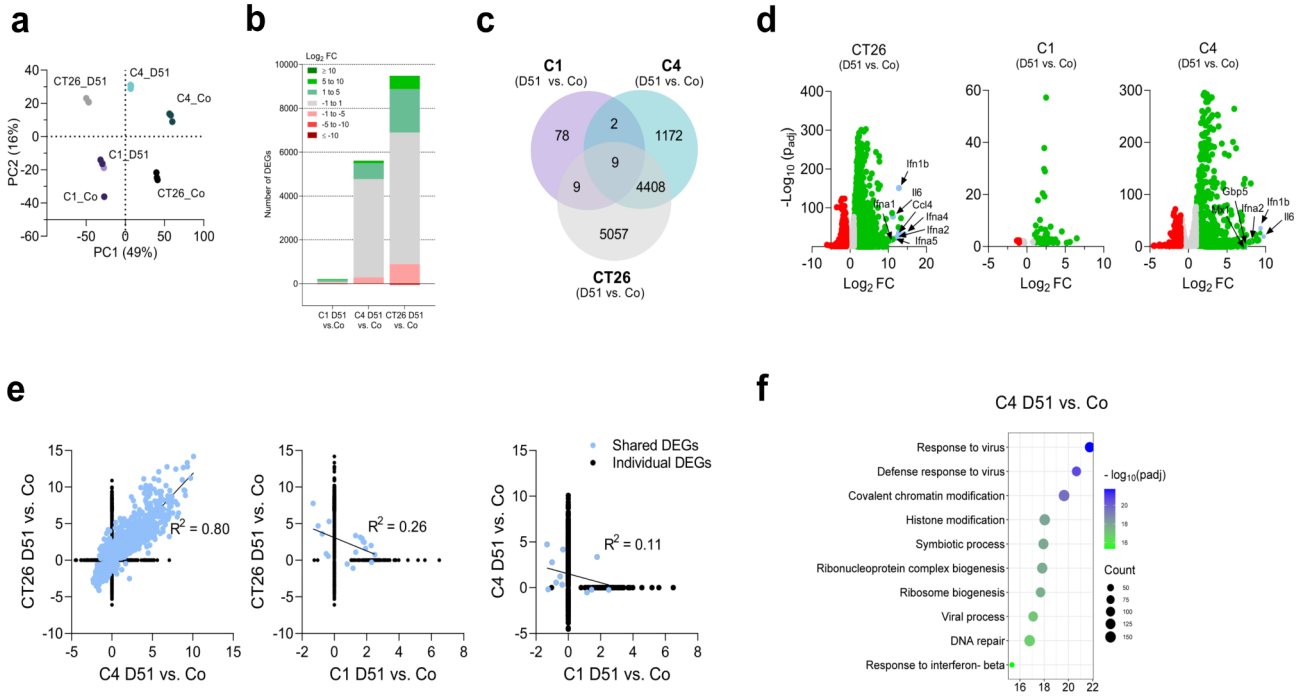

Fig. 5. Transcriptomic differences in C1 and C4 after VSV-D51 infection. (**a**) Principal component analysis of the overall gene expression in naïve CT26, C1, and C4 infected (D51) and uninfected (Co) cells. **(b)** Distribution of DEGs in infected vs. uninfected cells in C1 (C1 D51 vs. Co), C4 (C4 D51 vs. Co), and naïve CT26 cells (CT26 D51 vs. Co), with statistical significance ($P_{adj} < 0.05$). **(c)** Venn diagram of the differentially co-expressed genes (C1, C4 and naïve CT26 infected vs. their uninfected controls). **(d)** Volcano plot of differentially expressed genes in pairwise comparisons (C1, C4 and naïve CT26 infected vs. uninfected). Some strongly overexpressed genes in C4 and CT26-infected cells are marked with arrows (See also Supplementary Tables S3-S5). **(e)** Correlation in pairwise comparisons of total (individual DEGs) and shared DEGs. R^2 values indicate the goodness of fit of the shared DEGs linear regression (C4/CT26, $P < 0.001$; C1/CT26, $P < 0.05$; C1/C4, $P > 0.05$). **(f)** GO enrichment analysis of the top 10 enriched biological processes in C4 infected vs. uninfected cells.

activation of antiviral immunity is a potent mechanism of resistance to oncolytic VSV in different types of tumor cells[6,16,33,34].

In C4 and naïve CT26 cells, the cellular response to VSV infection was marked by the massive overexpression of IFN-related and antiviral gene expression patterns, which were not constitutively expressed, ruling out chronic immune activation as the cause of VSV resistance. Although both cell populations responded to VSV infection by activating innate immunity pathways, naïve CT26 cells showed a more extensive gene reprogramming response compared to C4, along with a diminished ability to respond to exogenous stimulation of the antiviral signaling. Comparison between basal transcriptomics in C4 and naïve CT26 revealed that C4 was overstimulating processes related to cytoskeletal reorganization, cell morphogenesis, and small-GTPase signal transduction, without significantly enhancing any immune-related gene expression, suggesting that cellular structural changes may underlie its partial susceptibility to VSV infection. Although chronic activation of the immune response has been shown to be a general resistance mechanism applicable to other VSV variants and viruses[6,12], cytoskeletal reorganization is a dynamic process that can reduce susceptibility to infection through various mechanisms, as VSV recruits actin and other cytoskeletal components for both entry and internalization[35,36], intracellular transport[37,38], and viral egress. Concerning the C1-resistance phenotype, the heterogeneous behavior of the CT26 line regarding susceptibility to VSV-D51 and IFN-I response has been previously demonstrated, as Ruotsalainen et al.[17] described the opposite behavior of two CT26 clones against IFN-I response. The B16-F10 line, from which we also isolated highly resistant clones, had previously demonstrated its ability to escape to oncolytic VSV infection by increasing IFN-I signaling[39]. On the other hand, VSV susceptibility can be limited by altering viral entry pathways, disrupting intracellular transport, or limiting the active diffusion of viral components[40–42]. Therefore, both chronic immune response and cytoskeletal control fall within the spectrum of cellular evasion strategies against VSV infection.

Both resistant clones were less susceptible to VSV-D51 than naïve CT26 cells, but only C1 showed reduced viral titers and RNA levels during wild-type VSV infection, suggesting a role of M residue 51 in cellular resistance for clone C4. The best characterized cellular interactor of the M protein is the Rae1/Nup98 complex, since this leads to the physical blockade of the nuclear pore complex and triggers a general inhibition of mRNA nuclear export[43]. The D51 variant of M cannot perform this blockade, leading to the activation of many genes in response to infection. We hypothesize that in C4 cells, the combination of basally deregulated genes and those activated

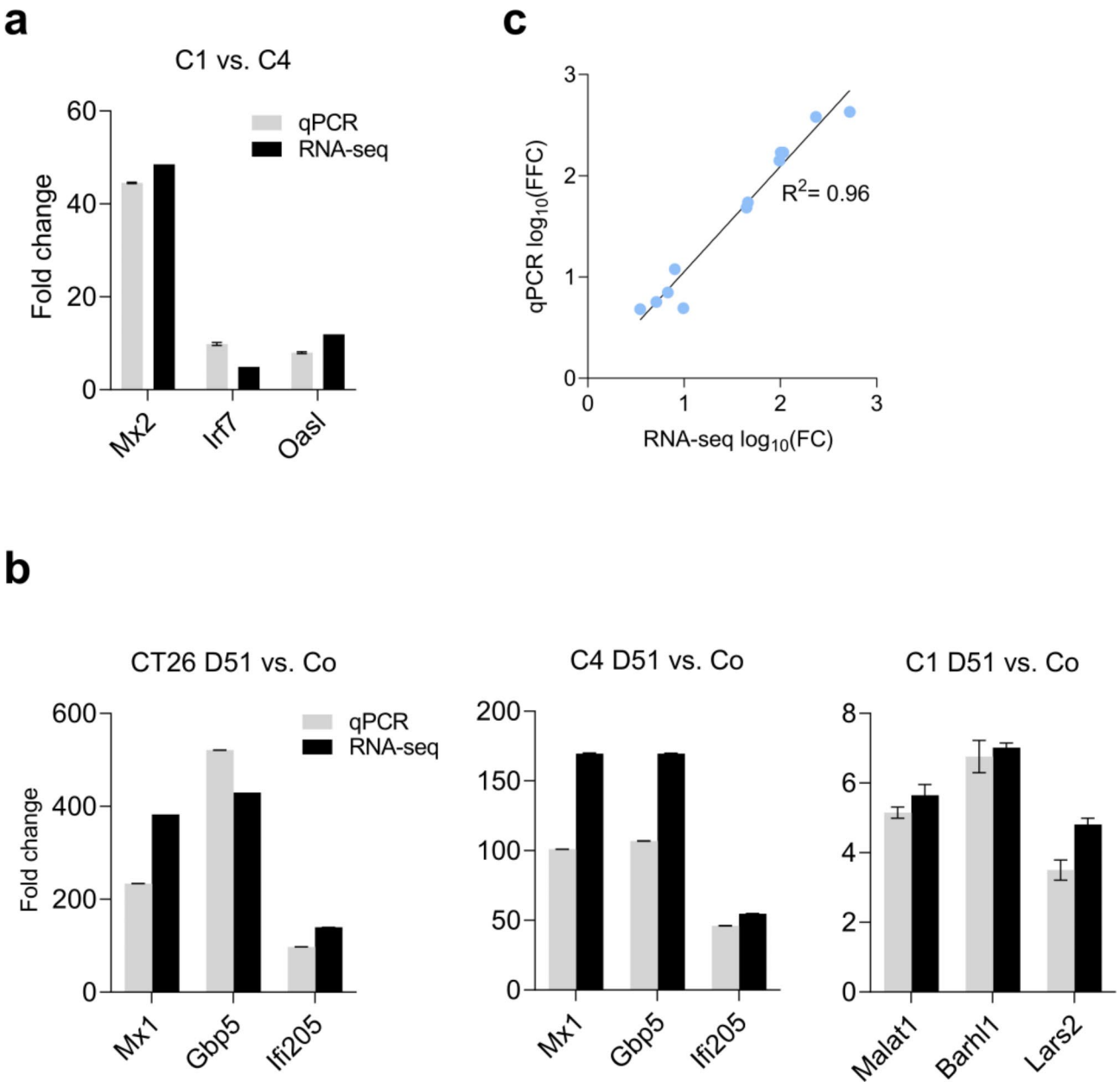

Fig. 6. RT-qPCR validation of the RNAseq. (**a**) Comparison between RNA-seq and qPCR data results for differentially expressed genes in C1 vs. C4 cells (uninfected). (**b**) Comparison of RNA-seq and qPCR data for differentially expressed genes in C1, C4 and naïve CT26 infected with VSV-D51 vs. uninfected (Co) samples. (**c**) Correlation between RNA-seq and qPCR data.

by D51 infection may confer resistance, whereas the inability to activate additional genes during wild-type VSV infection did not result in resistance. In contrast, since C1 were primed against infection by activation of innate immunity, they became less susceptible to both VSV-D51 and wild-type VSV.

Predictive models for the interaction of M mutants with cell targets may be valuable when M retains part of its mRNA export inhibitory function. This type of work was performed by Morris et al.[44] with substitution D52G in the M protein, which allows activation of the NF-kB signaling pathway but not IFN production. We searched for VSV M interactors in the p-HIPSTer[45] and IntAct[46] databases that were dysregulated in C1 or C4 cells. This was the case for human MAGI1 (UniProt: Q96QZ7) and WWTR1 (Q9GZV5), whose orthologs showed slightly reduced expression in C4 cells, although residue 51 did not appear to be involved in this interaction[47]. Human NDUFAF4 (Q9P032) has also been reported to be an M-interactor, and the shutdown of this gene promotes VSV replication independent of IFN activation[48]. The slight reduction in *Ndufaf4* expression in C4 ($\log_2$ fold change of −0.32) may contribute to the VSV-resistant phenotype, warranting experimental validation.

Although cell cultures are simplified systems for study infection susceptibility, current approaches such as single-cell transcriptomic sequencing have demonstrated that intrapopulation heterogeneity is a shared feature

of both normal and tumor cell lines[49–56]. Intrapopulation heterogeneity can manifest through differential intra-regulation of cellular processes such as cell cycle, senescence, stress, interferon response, and permissiveness to viral infection[57]. Understanding virus-host interactions could lead to the development of more effective strategies to overcome resistance and improve the efficacy of VSV-based cancer treatments[58]. A VSV clinical candidate with a modified glycoprotein from the choriomeningitis virus (VSV-GP) is currently undergoing human trials (NCT05155332, NCT05839600). VSV-IFNβ-NIS, engineered to express interferon-beta (IFN-β) and the sodium iodide symporter (NIS), also demonstrated therapeutic potential and is in trials alone and in combination with other treatments (NCT03017820, NCT06508463, and NCT03647163). Comparative transcriptomic studies between cells infected by these and other VSV candidates sensitive to IFN-I signaling would be valuable for identifying resistance gene signatures that could have clinical relevance[59]. The study of resistance signatures in vivo remains crucial to advance our understanding of the unresponsiveness to oncolytic therapies. Although the impact of antiviral signaling on oncolytic therapy outcomes has been further documented[12], structural cellular resistances have not been fully evaluated. This study underscores the multifaceted nature of VSV susceptibility in CT26 cells, revealing the critical role of transcriptional differences, and suggesting the presence of multiple cellular mechanisms that orchestrate resistance.

Methods

Viruses

Wild-type (VSV-WT-mCherry) and oncolytic VSV (VSV-D51-GFP) viruses of the Indiana serotype were kindly provided by Dr. Valery Z. Grdzelishvili (University of North Carolina, CA, USA). The reporter genes (GFP and mCherry) were located in the intergenic region between the G and L genes.

Cell lines

CT26 (CVCL-7255) and BHK-21 (CVCL_0159) cells were obtained from the American Type Culture Collection (ATCC) and cultured in Dulbecco's Modified Eagle Medium (DMEM) supplemented with 10% fetal bovine serum (FBS), 1% non-essential amino acids, 50 U/mL penicillin, and 50 µg/mL streptomycin. Information regarding the gender or exact age of the source animals was not available. All cell lines and derived CT26 subpopulations were cultured at 37 °C under 95% humidity and 5% CO_2, and regularly subjected to mycoplasma contamination testing by PCR.

Virus titration by plaque assay

Viral titers were determined by plaque assay and expressed as plaque-forming units (PFU) per mL. For this, BHK-21 monolayers (90–95% cell confluence) were inoculated with serially diluted virus suspensions under standard culture conditions (37 °C, 5% CO_2) and overlaid with DMEM supplemented with 2% FBS and 0.5% agar after 45 min. After 20–24 h post-infection, solidified media was removed, and cells were fixed with 10% formaldehyde. Cells were stained with 2% crystal violet in 10% formaldehyde to visualize plaques.

Monolayer infections and viral infection tracking

Cell monolayers (90–95% confluence) were inoculated with the virus at the indicated multiplicity of infection (MOI), defined as the PFU/cell ratio. Real-time live-cell fluorescence imaging was performed using an IncuCyte S3 live-cell analysis system (Sartorious). Images were acquired using phase contrast, green and red channels with a 4X objective. Image analysis masks were calibrated using representative images at various time points and experimental conditions. Virus-induced cell death kinetics were assessed by measuring changes in cell confluence following infection. Phase contrast analysis masks estimated cell confluence as the percentage of cells remaining adhered to the monolayer. Cell detachment was observed in infected populations but not in uninfected controls, indicating that it was caused by virus-induced cell death.

Cell sorting

Confluent monolayers of CT26 cells were inoculated with VSV-D51 at a multiplicity of infection (MOI) of 5 PFU/cell. At 24 hpi, dead cells were washed with phosphate-buffered saline (PBS), survivor cells were allowed to regrow for 72 h, and the whole process was repeated twice. After the final round of infection, cells were washed with PBS, allowed to recover for 24 h, detached from the plate using trypsin-EDTA, resuspended in PBS + 10% FBS, and prepared for flow cytometry as described previously[16]. Approximately one million events were analyzed, and naïve CT26 populations were used to identify surviving GFP-negative CT26 cells. Cells were sorted using a Beckman Coulter "MoFlo Legacy" cell sorter into 96-well plates, amplified by serial transfer to 100 mm plates, and finally stored at -150 °C. Initially, we seeded 48 individual cells, but only five managed to grow to form new populations. Two of the five clones, named C1 and C4, were free of VSV as determined by RT-qPCR.

RT-qPCR

Media from infected cells (6-well confluent monolayers) were removed, and total (cellular and viral) RNA was extracted using RNAzol RT (Sigma-Aldrich) following the manufacturer's instructions. Reverse transcription (RT) was carried out using M-MuLV reverse transcriptase (NZYtech) at 50 °C using specific primers. Subsequently, quantitative PCR (qPCR) was performed using the PowerUP SYBR Green qPCR Master Mix (Applied Biosystems) in a Quant Studio 3.0 qPCR thermocycler (Applied Biosystems). The thermal profile used was 95 °C for 10 min, followed by 40 cycles at 95 °C for 5 s, 55 °C for 1 min, and 60 °C for 20 s. Melting curve analysis was used to check for the absence of primer dimers, non-specific amplifications, and contaminating cDNA in the master mixes. Additionally, no-RT and no-template controls were included. To detect viral replication, the VSV-L gene was subjected to RT using a plus-strand primer, whereas oligodT was used for total

cellular mRNAs. For qPCR, primers for VSV-L gene and β-actin were chosen. Nine differentially regulated cellular genes (*Mx2*, *Irf7*, *Oasl*, *Malat1*, *Barhl1*, *Lars2*, *Mx1*, *Gbp5* and *Ifi205*) were selected for the validation of the RNAsequencing (RNA-seq) results, and *β-actin* was chosen as the reference gene. The relative expression of the selected genes was normalized using the Pfaffl method[60]. Primer sequences for all genes are listed in Supplementary Table S1.

RNA sequencing

Confluent monolayers were seeded and infected in triplicate with VSV-D51 at MOI = 1 PFU/cell. After 45 min, the viral inoculum was removed and infected and uninfected cells were filled with complete 1X DMEM. At 8 hpi, the media was aspirated and each monolayer was collected separately using RNAzol RT (Sigma Aldrich). Total RNA was extracted according to the manufacturer's instructions. The samples were quantified and checked for A260/280 and A260/230 quality ratios (> 1.9). Integrity quality analysis was performed in-house using Agilent 2100 Bioanalyzer and externally (Novogene, Cambridge, UK). To enrich and purify mRNA from total RNA, poly-T oligo-attached magnetic beads were utilized. Following fragmentation, first-strand cDNA was synthesized using random hexamer primers and second-strand cDNA was synthesized using dTTP for a non-directional library. The size distribution of the libraries was quantified using absorbance (Qubit) and qPCR. Illumina NovaSeq 6000 platform was used to sequence the library preparations, generating approximately 150 base paired-end raw reads. Raw reads in FASTQ format were first processed using fastp (v0.23.0). The obtained clean reads were mapped to the *Mus musculus* genome using HISAT2 (v2.0.5) with default parameters. Featurecounts (v1.5.0-p3) was used to obtain read counts and fragments per kilobase per million mapped reads (FPKM). Read quality and mapping data are provided in Supplementary Table S2. DESeq2 (v1.20.0) was used to identify differentially expressed genes (DEGs) in pairwise comparisons, adjusting the P-values to the Benjamini and Hochberg correction for false discovery rate (FDR), and selecting those with a P-adjusted value (P_{adj}) < 0.05. Principal component analyses (PCA) were performed in R using variance-stabilizing-transformation (VST) normalization of read counts. Hierarchical heatmaps and cluster analyses were performed using iDEP[61] and SRplot[62]. Gene Ontology (GO) and Kyoto Encyclopedia of Genes and Genomes (KEGG)[63] functional analysis were performed using ClusterProfiler (v4.8.3), iDEP and gProfiler[64], and using Benjamini and Hochberg correction for FDR < 0.25 and selected the P_{adj} < 0.05 terms.

Statistics

All viral infections were performed in triplicate, and the values are reported as the mean ± SEM for each case. Graphs and statistical analyses were performed in GraphPad Prism 8, and significance thresholds for all statistical tests were: *** $P < 0.001$; ** $P < 0.01$; * $P < 0.05$; ns: not significant. Data management was performed using RStudio (R version 4.4.1).

Data availability

The raw sequences of VSV-D51 infected C1, C4 and naïve CT26 cells were deposited in the NCBI Short Read Archive (SRA) database and added to the BioProject accession number PRJNA855353. All unique reagents (C1 and C4 clones and VSV constructs) developed and/or used in this study are available upon request (rafael.sanjuan@uv.es).

Received: 12 June 2024; Accepted: 30 October 2024
Published online: 08 November 2024

References

1. Huang, Z. et al. Application of oncolytic virus in tumor therapy. *J Med Virol* 95. (2023). https://doi.org/10.1002/jmv.28729
2. Kaufman, H. L., Kohlhapp, F. J. & Zloza, A. Oncolytic viruses: a new class of immunotherapy drugs. *Nat. Rev. Drug Discov.* **14**, 642–662. https://doi.org/10.1038/nrd4663 (2015).
3. Hemminki, O., dos Santos, J. M. & Hemminki, A. Oncolytic viruses for cancer immunotherapy. *J. Hematol. Oncol.* **13**, 84. https://doi.org/10.1186/s13045-020-00922-1 (2020).
4. Volovat, S. R. et al. Oncolytic Virotherapy: a New Paradigm in Cancer Immunotherapy. *Int. J. Mol. Sci.* **25**, 1180. https://doi.org/10.3390/ijms25021180 (2024).
5. Buijs, P. R., Verhagen, J. H., van Eijck, C. H. & van den Hoogen, B. G. Oncolytic viruses: from bench to bedside with a focus on safety. *Hum. Vaccin Immunother.* **11**, 1573–1584. https://doi.org/10.1080/21645515.2015.1037058 (2015).
6. Ebrahimi, S. et al. Interferon-mediated Tumor Resistance to Oncolytic Virotherapy. *J. Cell. Biochem.* **118**, 1994–1999. https://doi.org/10.1002/jcb.25917 (2017).
7. Budhwani, M., Mazzieri, R. & Dolcetti, R. Plasticity of type I Interferon-mediated responses in Cancer Therapy: from anti-tumor immunity to resistance. *Front. Oncol.* **8** https://doi.org/10.3389/fonc.2018.00322 (2018).
8. Wu, Y. et al. Histone Deacetylase Inhibitor Panobinostat Benefits the Therapeutic Efficacy of Oncolytic Herpes Simplex Virus Combined with PD-1/PD-L1 Blocking in Glioma and Squamous Cell Carcinoma Models. *Viruses* 14, 2796. (2022). https://doi.org/10.3390/v14122796
9. Chen, R. et al. The application of histone deacetylases inhibitors in glioblastoma. *J. Exp. Clin. Cancer Res.* **39**, 138. https://doi.org/10.1186/s13046-020-01643-6 (2020).
10. Tong, J. G. et al. Spatial and temporal epithelial ovarian cancer cell heterogeneity impacts Maraba virus oncolytic potential. *BMC Cancer.* **17**, 594. https://doi.org/10.1186/s12885-017-3600-2 (2017).
11. Berg, D. R. et al. In vitro and in silico multidimensional modeling of oncolytic tumor virotherapy dynamics. *PLoS Comput. Biol.* **15**, e1006773. https://doi.org/10.1371/journal.pcbi.1006773 (2019).
12. Bhatt, D. K., Chammas, R. & Daemen, T. Resistance mechanisms influencing Oncolytic Virotherapy, a systematic analysis. *Vaccines (Basel).* **9**, 1166. https://doi.org/10.3390/vaccines9101166 (2021).
13. Stojdl, D. F. et al. Exploiting tumor-specific defects in the interferon pathway with a previously unknown oncolytic virus. *Nat. Med.* **6**, 821–825. https://doi.org/10.1038/77558 (2000).
14. Escobar-Zarate, D., Liu, Y. P., Suksanpaisan, L., Russell, S. J. & Peng, K. W. Overcoming cancer cell resistance to VSV oncolysis with JAK1/2 inhibitors. *Cancer Gene Ther.* **20**, 582–589. https://doi.org/10.1038/cgt.2013.55 (2013).

15. Saloura, V. et al. Evaluation of an attenuated vesicular stomatitis Virus Vector Expressing Interferon-β for Use in Malignant Pleural Mesothelioma: heterogeneity in Interferon Responsiveness defines potential efficacy. *Hum. Gene Ther.* **21**, 51–64. https://doi.org/10.1089/hum.2009.088 (2010).
16. Larrieux, A. & Sanjuán, R. Cellular resistance to an oncolytic virus is driven by chronic activation of innate immunity. *iScience*. **26**, 105749. https://doi.org/10.1016/j.isci.2022.105749 (2023).
17. Ruotsalainen, J. J. et al. Clonal variation in interferon response determines the outcome of oncolytic virotherapy in mouse CT26 colon carcinoma model. *Gene Ther.* **22**, 65–75. https://doi.org/10.1038/gt.2014.83 (2015).
18. Holbrook, M. C., Goad, D. W. & Grdzelishvili, V. Z. Expanding the spectrum of pancreatic cancers responsive to vesicular stomatitis virus-based oncolytic virotherapy: challenges and solutions. *Cancers (Basel)*. **13**, 1171. https://doi.org/10.3390/cancers13051171 (2021).
19. Hastie, E., Cataldi, M., Marriott, I. & Grdzelishvili, V. Z. Understanding and altering cell tropism of vesicular stomatitis virus. *Virus Res.* **176**, 16–32. https://doi.org/10.1016/j.virusres.2013.06.003 (2013).
20. Stojdl, D. F. et al. VSV strains with defects in their ability to shutdown innate immunity are potent systemic anti-cancer agents. *Cancer Cell.* **4**, 263–275. https://doi.org/10.1016/S1535-6108(03)00241-1 (2003).
21. Rieder, M. & Conzelmann, K. K. Rhabdovirus evasion of the interferon system. *J. Interferon Cytokine Res.* **29**, 499–509. https://doi.org/10.1089/jir.2009.0068 (2009).
22. Al-Zaher, A., Domingo-Calap, P. & Sanjuán, R. Experimental virus evolution in cancer cell monolayers, spheroids, and tissue explants. *Virus Evol.* **7** https://doi.org/10.1093/ve/veab045 (2021).
23. Moerdyk-Schauwecker, M. et al. Resistance of pancreatic cancer cells to oncolytic vesicular stomatitis virus: role of type I interferon signaling. *Virology*. **436**, 221–234. https://doi.org/10.1016/j.virol.2012.11.014 (2013).
24. Bishnoi, S., Tiwari, R., Gupta, S., Byrareddy, S. & Nayak, D. Oncotargeting by vesicular stomatitis Virus (VSV): advances in Cancer Therapy. *Viruses*. **10**, 90. https://doi.org/10.3390/v10020090 (2018).
25. Bykov, Y., Dawodu, G., Javaheri, A., Garcia-Sastre, A. & Cuadrado-Castano, S. Immune responses elicited by ssRNA(-) oncolytic viruses in the host and in the tumor microenvironment. *J. Cancer Metastasis Treat.* **9** https://doi.org/10.20517/2394-4722.2022.92 (2023).
26. Ruotsalainen, J. et al. Interferon-β sensitivity of Tumor cells correlates with poor response to VA7 Virotherapy in Mouse Glioma models. *Mol. Ther.* **20**, 1529–1539. https://doi.org/10.1038/mt.2012.53 (2012).
27. Liikanen, I. et al. Induction of Interferon pathways mediates in vivo resistance to Oncolytic Adenovirus. *Mol. Ther.* **19**, 1858–1866. https://doi.org/10.1038/mt.2011.144 (2011).
28. Paglino, J. C. & van den Pol, A. N. Vesicular stomatitis Virus has extensive oncolytic activity against human sarcomas: Rare Resistance is overcome by blocking Interferon pathways. *J. Virol.* **85**, 9346–9358. https://doi.org/10.1128/jvi.00723-11 (2011).
29. Huang, P. Y., Guo, J. H. & Hwang, L. H. Oncolytic sindbis virus targets tumors defective in the Interferon Response and induces significant bystander antitumor immunity in vivo. *Mol. Ther.* **20**, 298–305. https://doi.org/10.1038/mt.2011.245 (2012).
30. Cataldi, M., Shah, N. R., Felt, S. A. & Grdzelishvili, V. Z. Breaking resistance of pancreatic cancer cells to an attenuated vesicular stomatitis virus through a novel activity of IKK inhibitor TPCA-1. *Virology*. **485**, 340–354. https://doi.org/10.1016/j.virol.2015.08.003 (2015).
31. Dold, C. et al. Application of interferon modulators to overcome partial resistance of human ovarian cancers to VSV-GP oncolytic viral therapy. *Mol. Ther. Oncolytics*. **3**, 16021. https://doi.org/10.1038/mto.2016.21 (2016).
32. Felt, S. A., Droby, G. N. & Grdzelishvili, V. Z. Ruxolitinib and Polycation Combination Treatment overcomes multiple mechanisms of resistance of pancreatic Cancer cells to oncolytic vesicular stomatitis virus. *J. Virol.* **91**, e00461–e00417. https://doi.org/10.1128/jvi.00461-17 (2017).
33. Liu, Y. P., Suksanpaisan, L., Steele, M. B., Russell, S. J. & Peng, K. W. Induction of antiviral genes by the tumor microenvironment confers resistance to virotherapy. *Sci. Rep.* **3** https://doi.org/10.1038/srep02375 (2013).
34. Vähä-Koskela, M. & Hinkkanen, A. Tumor restrictions to Oncolytic Virus. *Biomedicines*. **2**, 163–194. https://doi.org/10.3390/biomedicines2020163 (2014).
35. Cureton, D. K., Massol, R. H., Saffarian, S., Kirchhausen, T. L. & Whelan, S. P. J. Vesicular stomatitis Virus enters cells through vesicles incompletely coated with clathrin that depend upon actin for internalization. *PLoS Pathog.* **5**, e1000394. https://doi.org/10.1371/journal.ppat.1000394 (2009).
36. Belot, L., Albertini, A. & Gaudin, Y. Structural and cellular biology of rhabdovirus entry. *Adv. Virus Res.* **104**, 147–183. https://doi.org/10.1016/bs.aivir.2019.05.003 (2019).
37. Yacovone, S. K. et al. Migration of Nucleocapsids in vesicular stomatitis virus-infected cells is dependent on both microtubules and actin filaments. *J. Virol.* **90**, 6159–6170. https://doi.org/10.1128/JVI.00488-16 (2016).
38. Heinrich, B. S., Cureton, D. K., Rahmeh, A. A. & Whelan, S. P. J. Protein expression redirects vesicular stomatitis Virus RNA synthesis to cytoplasmic inclusions. *PLoS Pathog.* **6**, e1000958. https://doi.org/10.1371/journal.ppat.1000958 (2010).
39. Huff, A. L. et al. APOBEC3 mediates resistance to oncolytic viral therapy. *Mol. Ther. Oncolytics*. **11**, 1–13. https://doi.org/10.1016/j.omto.2018.08.003 (2018).
40. Taylor, M. P., Koyuncu, O. O. & Enquist, L. W. Subversion of the actin cytoskeleton during viral infection. *Nat. Rev. Microbiol.* **9**, 427–439. https://doi.org/10.1038/nrmicro2574 (2011).
41. Moran, S. J. et al. Dynamic actin filament traps mediate active diffusion of vesicular stomatitis Virus Ribonucleoproteins. *J. Virol.* **96** https://doi.org/10.1128/jvi.00934-22 (2022).
42. Moran, S. J. et al. Mechanisms of active diffusion of vesicular stomatitis virus inclusion bodies and cellular early endosomes in the cytoplasm of mammalian cells. *PLoS One*. **19**, e0290672. https://doi.org/10.1371/journal.pone.0290672 (2024).
43. Faria, P. A. et al. VSV disrupts the Rae1/mrnp41 mRNA Nuclear Export Pathway. *Mol. Cell.* **17**, 93–102. https://doi.org/10.1016/j.molcel.2004.11.023 (2005).
44. Morris, M. C. et al. Computational prediction of intracellular targets of wild-type or mutant vesicular stomatitis matrix protein. *PLoS One*. **17**, e0263065. https://doi.org/10.1371/journal.pone.0263065 (2022).
45. Lasso, G. et al. A structure-informed atlas of human-virus interactions. *Cell*. **178**, 1526–1541e16. https://doi.org/10.1016/j.cell.2019.08.005 (2019).
46. Orchard, S. et al. The MIntAct project—IntAct as a common curation platform for 11 molecular interaction databases. *Nucleic Acids Res.* **42**, D358–D363. https://doi.org/10.1093/nar/gkt1115 (2014).
47. Mihalič, F. et al. Large-scale phage-based screening reveals extensive pan-viral mimicry of host short linear motifs. *Nat. Commun.* **14**, 2409. https://doi.org/10.1038/s41467-023-38015-5 (2023).
48. Pan, W., Shen, Z., Wang, H. & He, H. The host cellular protein Ndufaf4 interacts with the vesicular stomatitis virus M protein and affects viral propagation. *Virus Genes*. **57**, 250–257. https://doi.org/10.1007/s11262-021-01833-0 (2021).
49. Wu, F. et al. Single-cell profiling of tumor heterogeneity and the microenvironment in advanced non-small cell lung cancer. *Nat. Commun.* **12**, 2540. https://doi.org/10.1038/s41467-021-22801-0 (2021).
50. Zheng, H. et al. Single-cell analysis reveals cancer stem cell heterogeneity in hepatocellular carcinoma. *Hepatology*. **68**, 127–140. https://doi.org/10.1002/hep.29778 (2018).
51. Shen, Y. et al. Detecting heterogeneity in and between breast cancer cell lines. *Cancer Converg.* **4**, 1. https://doi.org/10.1186/s41236-020-0010-1 (2020).
52. Marusyk, A., Janiszewska, M. & Polyak, K. Intratumor Heterogeneity: the Rosetta Stone of Therapy Resistance. *Cancer Cell.* **37**, 471–484. https://doi.org/10.1016/j.ccell.2020.03.007 (2020).

53. Sun, X. & Yu, Q. Intra-tumor heterogeneity of cancer cells and its implications for cancer treatment. *Acta Pharmacol. Sin.* **36**, 1219–1227. https://doi.org/10.1038/aps.2015.92 (2015).
54. Kinker, G. S. et al. Pan-cancer single-cell RNA-seq identifies recurring programs of cellular heterogeneity. *Nat. Genet.* **52**, 1208–1218. https://doi.org/10.1038/s41588-020-00726-6 (2020).
55. Rahimi, A. M., Cai, M. & Hoyer-Fender, S. Heterogeneity of the NIH3T3 Fibroblast Cell Line. *Cells* 11, 2677. (2022). https://doi.org/10.3390/cells11172677
56. Català, P., Groen, N., LaPointe, V. L. S. & Dickman, M. M. A single-cell RNA-seq analysis unravels the heterogeneity of primary cultured human corneal endothelial cells. *Sci. Rep.* **13**, 9361. https://doi.org/10.1038/s41598-023-36567-6 (2023).
57. Shalek, A. K. et al. Single-cell RNA-seq reveals dynamic paracrine control of cellular variation. *Nature*. **510**, 363–369. https://doi.org/10.1038/nature13437 (2014).
58. Lin, C. et al. Immune landscape and response to oncolytic virus-based immunotherapy. *Front. Med.* **18**, 411–429. https://doi.org/10.1007/s11684-023-1048-0 (2024).
59. Hastie, E. & Grdzelishvili, V. Z. Vesicular stomatitis virus as a flexible platform for oncolytic virotherapy against cancer. *J. Gen. Virol.* **93**, 2529–2545. https://doi.org/10.1099/vir.0.046672-0 (2012).
60. Pfaffl, M. W. A new mathematical model for relative quantification in real-time RT-PCR. *Nucleic Acids Res.* **29**, 45e–445. https://doi.org/10.1093/nar/29.9.e45 (2001).
61. Ge, S. X., Son, E. W. & Yao, R. iDEP: an integrated web application for differential expression and pathway analysis of RNA-Seq data. *BMC Bioinform.* **19**, 534. https://doi.org/10.1186/s12859-018-2486-6 (2018).
62. Tang, D. et al. SRplot: a free online platform for data visualization and graphing. *PLoS One*. **18**, e0294236. https://doi.org/10.1371/journal.pone.0294236 (2023).
63. Kanehisa, M. & Goto, S. K. E. G. G. Kyoto encyclopedia of genes and genomes. *Nucleic Acids Res.* **28**, 27–30. https://doi.org/10.1093/nar/28.1.27 (2000).
64. Kolberg, L. et al. G:profiler—interoperable web service for functional enrichment analysis and gene identifier mapping (2023 update). *Nucleic Acids Res.* **51**, W207–W212. https://doi.org/10.1093/nar/gkad347 (2023).

Acknowledgements

We thank María Durán-Moreno and Iván Andreu-Moreno for technical assistance.

Author contributions

Conceptualization, R.S.; Methodology, A.L. and R.S.; Research, A.L.; Data analysis, A.L. and R.S.; Resources, R.S.; Writing – Original Draft, A.L. and R.S.; Visualization, A.L. and R.S.; Supervision, R.S.; Funding acquisition, R.S.

Declarations

Competing interests

The authors declare no competing interests.

Additional information

Supplementary Information The online version contains supplementary material available at https://doi.org/10.1038/s41598-024-78313-6.

Correspondence and requests for materials should be addressed to R.S.

Reprints and permissions information is available at www.nature.com/reprints.

Publisher's note Springer Nature remains neutral with regard to jurisdictional claims in published maps and institutional affiliations.